polymer papers

Segregation behaviour of deuterated poly(styrene-*block*-methyl methacrylate) diblock copolymer in the presence of poly(methyl methacrylate) homopolymer

D. G. Bucknall* and J. S. Higgins†
Department of Chemical Engineering, Imperial College, London SW7 2BY, UK

and J. Penfold
Rutherford Appleton Laboratory, Chilton, Didcot, Oxon OX11 0QX, UK

and S. Rostami
Wilton Materials Research Centre, ICI plc, Wilton, Middlesbrough, Cleveland TS6 8JE, UK
(Received 23 March 1992; revised 9 July 1992)

Copolymer segregation behaviour has been studied using the technique of neutron critical reflection from layered samples. Surface segregation occurs due to location at the air/polymer interface of a copolymer microphase-segregated layer. Similar microphase segregation by the copolymer occurs during mutual diffusion with the homopolymer. By comparison with theoretical predictions, this segregation is shown to exhibit behaviour characteristic of end-tethered polymer brushes.

(Keywords: polystyrene; poly(methyl methacrylate); diblock copolymer; surface segregation; micelle formation; neutron reflection; deuterated copolymer)

INTRODUCTION

The surface composition of a condensed-phase blend has long been recognized to differ from that of the bulk. Recently, the effect of a surface on polymer blends has been investigated[1–5]. Much of this work has focused on the effect of isotopic labelling, which is used extensively to investigate polymer diffusion[6,7], polymer–polymer miscibility[8,9] and polymer chain conformations[10,11]. Such studies have utilized the differences in mass and neutron scattering cross-section between hydrogen and deuterium nuclei. However, it is now widely recognized that such isotopic blends do not mix in an ideal way. The polymers have a weak unfavourable Flory–Huggins interaction parameter χ_{ab}, and can be characterized by an upper critical solution temperature[5]. The presence of a free surface in such a polymeric isotopic blend has the effect of causing surface enrichment of the component with the lowest surface energy[2–4,12].

Similarly, the free surface can have profound influences on copolymers in homopolymer blends[1,13]. The activity of such copolymers is dependent on their chemical potential μ_c, and is generally limited by copolymer micelle formation within the homopolymer phase[1]. If the matrix homopolymer molecular weight is sufficiently high, the block copolymer micelles will segregate to pre-existing interfaces and by definition therefore to free surfaces[1,13]. A question as to the nature of the segregation mechanism therefore arises when the possibility for both isotopic and micellar effects are introduced into the system.

Several techniques have recently found applications to interfacial studies of polymeric systems. Typically a scattering cross-section or elemental composition is measured as a function of depth. The more powerful of these techniques utilize particle beams as the system probe. Both forward recoil spectroscopy[14] and nuclear reaction analysis (n.r.a.)[15] use He ion beams, while dynamic secondary-ion mass spectrometry (d.s.i.m.s.)[16] can use a variety of positive or negative ions to cause the sputtering necessary to the technique. However, these techniques have limited depth resolution and to a greater or lesser extent are all sample-destructive. The relatively newly developed technique of neutron reflection overcomes these shortfalls and provides higher depth resolution than is possible with the other techniques without causing damage to the sample. The information obtained in a neutron reflection experiment is the neutron refractive index as a function of depth normal to the reflection surface. By careful use of isotopic substitution, the technique therefore provides a sensitive probe of chemical composition profile normal to the surface. Neutron reflection is therefore an ideal technique for investigating the surface segregation of isotopically labelled copolymers in a homopolymer phase.

* Present address: Max-Planck-Institut für Polymerforschung, Postfach 3148, D-6500 Mainz, Germany
† To whom correspondence should be addressed

0032-3861/93/030451-08

NEUTRON REFLECTION

A full description of the theory of the neutron reflection (n.r.) technique can be found elsewhere[17,18]. Here we only outline the process of extracting a composition–depth profile from the experimentally obtained reflectivity–scattering vector data. At angles less than the critical angle θ_c, total reflection is observed and the reflectivity R—the ratio of reflected to incident beam intensities (I_r/I_i)—is equal to unity. At angles greater than θ_c the incident beam is both reflected and refracted into the sample, so that now $R<1$. The refracted beam can also be reflected from interfaces within the sample and emerges from the sample surface to combine with the other reflected beams to cause interference patterns. An interface within the sample will occur whenever there is a change of refractive index. It is therefore not difficult to see that the reflectivity curve (interference pattern) contains information on the refractive indices and layer thicknesses within the sample. It is not, in general, possible to obtain this information directly by inverting the reflectivity data. Analysis therefore often relies on calculating a model reflectivity curve using formalisms adapted from optics[19,20]. This model reflectivity curve is compared with the experimental data and the model modified until both experimental and simulated data match. With the possibility of multiple layers within the sample, a multilayer matrix method is often adopted for calculating reflectivities, since roughness/diffusivity can be conveniently introduced into the formalisms. The Abeles method[21] provides a suitable approach in which a characteristic matrix for each discrete layer is defined in terms of the Fresnel reflection coefficient:

$$r_{m,m+1}=\frac{(n_m \sin\theta_m - n_{m+1}\sin\theta_{m+1})}{(n_m \sin\theta_m + n_{m+1}\sin\theta_{m+1})}$$

and phase factor:

$$\beta_m=(2\pi/\lambda)n_m d_m \sin\theta$$

Once matrices for each individual layer have been calculated, an overall sample matrix is defined as the product of the individual layer matrices. The reflectivity is then simply related to the matrix elements of this sample matrix.

SURFACE SEGREGATION MECHANISMS

In a system consisting of diblock copolymers with homopolymers and in which some components are deuterated, there is the possibility of two mechanisms for surface segregation. One mechanism derives from the tendency of the copolymers to aggregate into micelles[1,13] and the other from isotopic surface enrichment[2–4]. For the system described in this paper, the diblock copolymer is itself deuterated, so that both mechanisms may be linked in the surface segregation behaviour of the copolymer.

Symmetric diblock copolymers consisting of A and B chains in a phase of A homopolymer will aggregate into spherical micelles if the concentration of the copolymer exceeds the critical micelle concentration (c.m.c.) in the A phase. The micelles formed will consist of a core of B chains surrounded, and thus shielded from the A matrix chains, by the A copolymer blocks. With the core and corona chains bonded, the corona can be considered as a polymer 'brush' grafted onto the core. It is the behaviour of these brushes that influences the micelle segregation behaviour via micelle–micelle interactions as well as micelle–interface and micelle–surface interactions[22]. The alternative view is that, above the c.m.c., copolymers form micelles that can themselves be considered as high-molecular-weight deuterated A polymers within a matrix of hydrogenated A homopolymers. In this case the surface-active behaviour of these copolymers will be influenced by isotopic enrichment mechanisms.

As long as the ratio of the degree of polymerization of homopolymer to that of the corona forming the copolymer block remains greater than unity, $N_A/N_C>1$, a dry brush situation exists between the micelle and homopolymer matrix. This is compared to the wet brush situation where $N_A/N_C\leqslant 1$. In this instance, electron microscopy and small-angle neutron scattering results of Kinning and coworkers[23] show that quite significant concentrations of the low-molecular-weight homopolymer are trapped within the core of the copolymer micelle and produce swelling of the corona. In contrast, for the dry brush situation only a small proportion of homopolymer chains are expected to penetrate into the corona and the core of the micelle, and consequently this leads to sharp interfaces between the various components[24]. Energetically, this is an unfavourable situation since the number of available polymer conformations is greatly reduced, resulting in an entropic increase to the free energy. By micellar segregation to the interfaces present within the system, the corona–homopolymer interfacial area is reduced, leading to a reduction in the overall free energy of the system. Micelle–micelle interactions are energetically favourable—within certain limits[22]—and cause aggregation at a surface or interface similar to deposition of atoms on a smooth surface[1]. This means that micelles will deposit preferentially at steps and will form a complete layer of micelles before the next layer begins to form. The shape of the brush formed by end-tethered chains can be treated theoretically using a mean-field approach[22]. Using such a treatment, the form of the brush shape can be described using a hyperbolic tangent function of the form[22].

$$\phi_c(z)=\frac{\phi_0}{2}\left[1+\tanh\left(\frac{2(z_{offset}-z)}{w}\right)\right] \qquad (1)$$

where ϕ_0 is the saturated copolymer volume fraction at the surface, i.e. $z=0$, and z_{offset} is the position where $\phi_0=1$. The denominator w is a width parameter, which is equal to the width of the overlap region between the matrix phase and the brush.

A mixture of a normal and a deuterated species at equilibrium can lead to an enriched surface of the deuterated component[2,25]. This arises from the enthalpic interactions between hydrogenated and deuterated molecules, which mix in a non-ideal way, and are influenced by the small difference in the polarizability between the C–H and C–D bonds[25]. In such cases, this difference in polarizability produces an unfavourable interaction between the two species and a slightly lower surface tension for the deuterated component. Mean-field theory predicts that, at equilibrium, there is an approximately exponential decay of the deuterated component volume fraction, from a high value at the surface, equal to ϕ_s, to its bulk value of ϕ_∞ (ref. 3). Associated with this profile is a decay length λ_d, which is of the order of the bulk correlation length for concentration fluctuations. Jones *et al.*[3] have

shown that this deuterated component volume fraction is described by the equation:

$$\phi(z)=(\phi_s-\phi_\infty)\exp[-(z/\lambda_d)^\xi]+\phi_\infty \quad (2)$$

where ξ is a dimensionless factor. At times less than that required to reach equilibrium, i.e. $t_a<t_{eq}$, the amount of deuterated polymer giving a surface excess of z_s^* is less than the equilibrium amount of $z_{s,eq}^*$. As the surface layer of deuterated component grows, so that z_s^* increases towards the equilibrium value, the surface layer removes material from an area behind it, causing a region depleted of the deuterated component. This situation is schematically illustrated in *Figure 1*. As deuterated material leaves the depleted region to enrich the surface layer, deuterated polymer from the bulk simultaneously diffuses down the concentration gradient into the depleted region to provide the material necessary for the continued growth of the surface layer.

The size of the depleted region is controlled by the diffusion distance $(Dt_a)^{1/2}$, where D is a mutual diffusion coefficient and t_a is the annealing time. The volume fraction of the depleted region nearest the surface layer, ϕ_d, can be considered to be in local equilibrium with the enriched layer, as it varies slowly in comparison with the diffusion distances associated with the enriched layer. Jones and Kramer[4] have shown that, using this local equilibrium as a boundary condition, the diffusion equation governing the supply of material to the surface enriched layer can be derived by combination of Fick's first and second laws. Alternatively, however, a simple approximate solution for the growth of this surface enriched layer can be derived by simple conservation-of-mass considerations. This dictates that the amount of material removed from the depleted region equals the surface excess. With the depleted region being of the order of $(Dt_a)^{1/2}$, and using the assumption, described above, that the depleted region is in local equilibrium with the surface layer, gives the approximate equality:[4]

$$z_s^*(t_a)=\frac{z_{s,eq}^*\phi_\infty(Dt_a)^{1/2}}{z_{s,eq}^*+\phi_\infty(Dt_a)^{1/2}} \quad (3)$$

Equation (3) shows that the surface layer grows with a $t_a^{1/2}$ dependence, which slows down as the equilibrium surface excess $z_{s,eq}^*$ is approached.

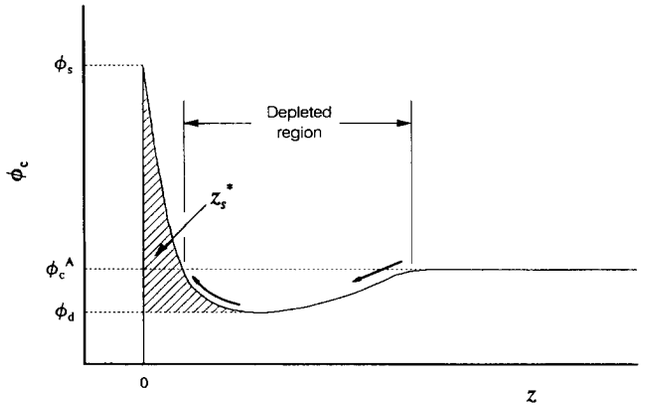

Figure 1 Schematic illustration of a non-equilibrium isotopically enriched surface layer, showing the depleted region and the diffusion path of the isotopic polymer

Table 1 Characteristics of the polymers used in this study

Polymer	Abbreviation	M_w	M_w/M_n
Poly(methyl methacrylate)[a]	PMMA	1.20×10^5	1.71
Deuterated poly(styrene-*block*-methyl methacrylate)[b]	dP(S-*b*-MMA)28	2.84×10^4	1.06

[a] Supplied by BDH
[b] Supplied by Polymer Laboratories

Table 2 Sample configurations, identification codes and cumulative annealing times. Configurations are labelled with the substrate (Sub) on the left

		Cumulative annealing times (min)	
Sample configurations	Code	$\Delta_1\pm5$	$\Delta_2\pm10$
Sub/dP(S-*b*-MMA)28/PMMA	δII	31	281
Sub/PMMA/dP(S-*b*-MMA)28	εII	250	–

EXPERIMENTAL

The characteristics of the polymers used in this work are listed in *Table 1*. The copolymer has a polystyrene (PS) segment with $M_w^{PS}=13\,300$ as determined by g.p.c. (data supplied by Polymer Laboratories, UK) and therefore a weight fraction of PS given by $f=0.47$. The individual polymer layers were prepared separately by spin casting from dilute toluene solutions, the concentrations of which varied between 0.4 and 2.5% wt/vol. The solutions were spun horizontally on a vacuum chuck spinner rotated at 1500–2000 r.p.m. The base layers of each sample were spun directly onto $\lambda/10$ optically polished glass substrates (25 mm radius × 10 mm thick), which had previously been washed with distilled water, toluene and acetone. The other polymer layers were spun onto large glass microscope slides (70 mm × 40 mm × 1 mm). After spinning, the films were placed in a vacuum oven at 40°C overnight. The polymer layers on the microscope slides were floated off onto the surface of distilled water and picked up onto the appropriate coated substrate. The samples were left to air-dry until no trapped water was visible under the top film, and then returned to the vacuum oven. The sample configurations prepared in this way are listed together with their identification codes in *Table 2*. The samples remained in the vacuum oven at 40°C for a period of a few days until required for the n.r. experiments. The n.r. profiles of each sample were measured in the 'as-made' (a.m.) state and also after annealing at 150±3°C for varying lengths of time. All reflectivity data presented in the following sections were recorded at room temperature on the CRISP 'TOF' (time-of-flight) reflectometer[26] at the ISIS facility, Rutherford Appleton Laboratory. From the a.m. sample reflectivities, dP(S-*b*-MMA)28 layer thicknesses were determined to be 330 and 313 Å for the samples δII and εII respectively. Similarly, PMMA layers 'as-made' were 1175 and 1150 Å thick, respectively, for these samples. The samples were annealed in an air atomsphere oven set at 150°C for the annealing times given in *Table 2*. Care was taken when measuring the Δ_1 and Δ_2 reflectivity profiles to align the sample in the same orientation as used for the 'as-made' sample measurement. This ensured that the reflectivity profile of the same section of the

polymer film was recorded in all cases. All the reduced raw time-of-flight data were analysed using semi-automatic fitting to produce the best visual fit with the lowest possible χ^2 parameter (a measure of the deviation from a perfect fit) and then checked for self-consistency. In other words, the model used to describe the reflection profile was tested to see if it was physically meaningful and then tested against a theory if available. In doing this analysis, it is necessary to convert the scattering length density (ρ_z) *versus* depth (z) profiles obtained from the fitting parameters into volume fraction (ϕ_k) *versus* depth (z) profiles. It is therefore possible to calculate on the basis of the 'as-made' sample whether the more complex ϕ_k *versus* z profiles of the annealed samples contain the same amounts of material.

RESULTS AND DISCUSSION

The reflectivity profiles of the δII sample were recorded in the 'as-made' (a.m.) state, and also after two annealing processes, Δ_1 and Δ_2 at 150°C (see *Table 2*). The reflectivity *versus* wavevector (Q) profiles for these samples are plotted together in *Figure 2*, where the profiles have been translated in the y axis for clarity. Error bars have also been omitted, first for clarity and secondly because for all but the highest Q values they are smaller than the size of the data points. Superimposed upon the data points of *Figure 2* are full curves representing the simplest simulated fits obtained from the analysis fitting routines described in the experimental section. Close agreement is observed at all values of Q between data and fits for both the δII a.m. and Δ_2 samples, and this is confirmed by the small value of χ^2.

The copolymer volume fraction ϕ_c as a function of the distance z from the air/polymer interface for the a.m. sample obtained from the fitting analysis model is shown by the broken lines in *Figure 3*. Analysis of the Δ_2 samples indicated by the full curve fitted to the data in *Figure 2* produced in the simplest case a four-layer model. On the basis that the layer immediately adjacent to the substrate with $\rho_z = 0.641 \times 10^{-5}$ Å^{-2} is pure copolymer, and assuming that $\rho_z(\text{PMMA}) = 0.11 \times 10^{-5}$ Å^{-2}, it is possible to determine the $\phi_c(z)$ profile of δIIΔ_2 from the data obtained from the fitting, using the general expression:

$$\rho_z = \rho_z(c)\phi_c + (1-\phi_c)\rho_z(k) \quad (4)$$

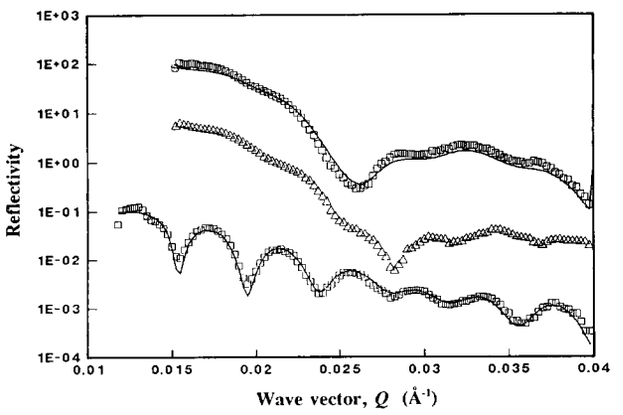

Figure 2 Reflectivity profiles for the δII sample 'as-made' (○), and after annealing for 31 min (△) and 281 min (□). The full curves superimposed upon the experimental data represent best-fit calculated reflectivity profiles, described in the text and *Figure 3*

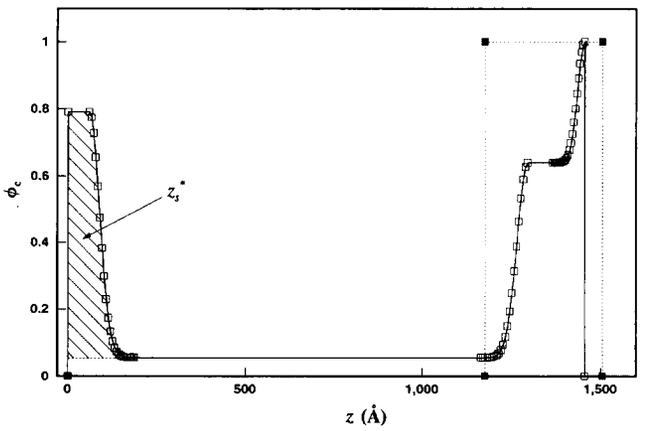

Figure 3 Copolymer volume fraction ϕ_c *versus* distance z from the free polymer surface for the sample δII 'as-made' (■) and Δ_2 (□), used to produce the best fits to the reflectivity profiles of *Figure 2*

where $\rho_z(c)$ and $\rho_z(k)$ denote the scattering length densities of the dP(S-*b*-MMA) copolymer and homopolymer k, respectively. The value of z is simply the total distance from the centre of the air/polymer interface and given by $z = \sum d_j$. Here d_j is the thickness of the jth layer, labelling from the air ($j=0$) to the substrate ($j=m+1$) for a sample with m layers. For sample δIIΔ_2, k = PMMA. The interfacial profiles between each layer were determined from the roughness parameter $z_{j,j+1}$, assuming half-Gaussian shapes where the standard deviation of the Gaussian $\sigma_G = z_{j,j+1}$. The ϕ_c *versus* z profile for the Δ_2 sample is plotted together with the a.m. profile in *Figure 3*.

Inspection of the $\phi_c(z)$ profile of Δ_2 in *Figure 3* shows that there are two areas of dP(S-*b*-MMA)28 segregation, at both the substrate/polymer interface and the air/polymer interface. The copolymer molecules at the substrate/polymer interface are the remnants of the initially pure layer of the a.m. sample, which through the action of mutual diffusion has formed a two-layer step profile. This profile is clearly not a simple Fickian diffusion profile, which can be described by an error function[27]. The presence of copolymer still attached to the substrate is likely to be due to the influence of hydrogen bonding between the carbonyl groups of the PMMA block of the copolymer and the hydroxyl groups present at the surface of the quartz. The formation of a step profile is discussed with preference to sample εIIΔ_1 in a later section. The surface enriched layer lying between $z=0$ and 180 Å has a surface excess value, defined as the area under the $\phi_c(z)$ curve, of $z_s^* = 78 \pm 10$ Å. This is shown by the hatched area in *Figure 3*. The surface excess is not pure copolymer as indicated by a ϕ_s value of 0.790 ± 0.005, which drops to a value in the PMMA bulk at $z \geqslant 180$ Å of $\phi_c^{\text{PMMA}} = 0.055 \pm 0.005$. As discussed previously, this surface segregated layer can be formed through either isotopic surface enrichment or micelle segregation mechanisms. Purely from the $\phi_c(z)$ profile it is unclear which of these mechanisms is responsible for this segregation—both possibilities are analysed in detail below.

Isotopic surface enrichment

Assuming that the copolymer surface segregated layer is formed via an isotopic enrichment mechanism, it is possible to apply the diffusion equations discussed above

to determine whether the system is at equilibrium. The equilibrium surface excess value $z^*_{s,eq}$ is obtained after a little rearrangement of equation (3). Substituting into equation (3) the appropriate values $\phi_\infty = \phi_c^{PMMA} = 0.055$, $z_s^* = 78$ Å and $t_a = 16\,860$ s, and using a mutual diffusion coefficient obtained from n.r.a. measurements[28], $D = D_{PMM} = 40\,Å^2\,s^{-1}$, gives an equilibrium surface excess value of $z^*_{s,eq} = 107 \pm 11$ Å. Therefore the value of $z_s^* = 78$ Å obtained experimentally is not an equilibrium quantity. Since sample $\delta II\Delta_2$ is not at equilibrium, a copolymer-depleted region would therefore be expected to exist just below the surface excess layer[4]. In the light of this, the four-layer fit discussed above was modified to include a depleted copolymer zone, giving a five-layer best fit as illustrated in *Figure 4*.

Using equation (4) the fitting parameters used to obtain the data fit in *Figure 4* can be converted to the ϕ_c *versus* z plot illustrated in *Figure 5*. Comparison with the four-layer fit of *Figure 3* shows that the $\phi_c(z)$ profiles at the substrate are effectively the same for both models. A difference is apparent only in the region directly behind the surface excess layer, where a region in the five-layer model extending between $z = 188$ and 428 Å has a reduced copolymer volume fraction, $\phi_d = 0.024 \pm 0.006$, from that in the bulk PMMA. By including a depleted layer the values of ϕ_c and ϕ_c^{PMMA} in the five-layer fit correspondingly increase to maintain the same total copolymer

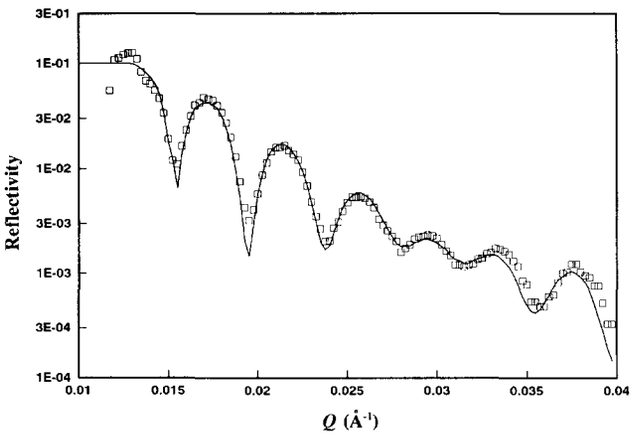

Figure 4 Reflectivity profile of fitting model (—) superimposed upon the $\delta II\Delta_2$ experimental data (□). The model assumes a depleted copolymer region immediately behind the copolymer surface segregated layer, as described by *Figure 5*

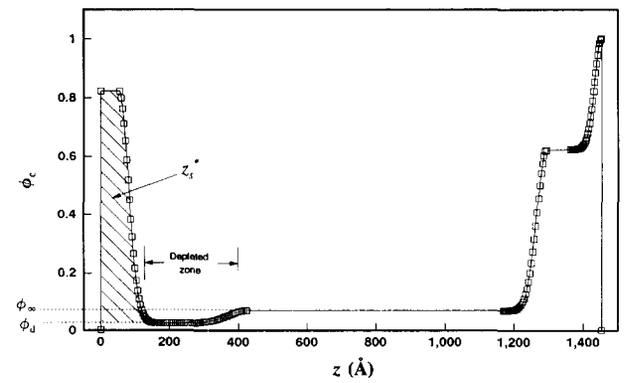

Figure 5 The $\phi_c(z)$ profile for the five-layer simulation model assuming a depleted copolymer region, giving the fit to the data in *Figure 4*

Table 3 Copolymer volume fractions obtained from the four- and five-layer simulated fits to the $\delta II\Delta_2$ profiles. Copolymer surface excess values are obtained from the area under the $\phi_c(z)$ profile of the surface layer, as shown in *Figures 3* and *5*

Quantity	Four-layer fit	Five-layer fit
ϕ_s	0.790 ± 0.005	0.83 ± 0.05
ϕ_d	–	0.024 ± 0.006
ϕ_c^{PMMA}	0.055 ± 0.005	0.068 ± 0.010
z_s^*	78 ± 10	69 ± 10

volume in the sample, so that $\phi_s = 0.83 \pm 0.05$ and $\phi_c^{PMMA} = 0.068 \pm 0.010$. The differences between the four- and five-layer simulated fits are summarized in *Table 3*. However, the five-layer fit is not visually as good as the corresponding four-layer fit, and the validity of the isotopic surface enrichment mechanism therefore becomes doubtful.

Jones *et al.*[3] have shown that, in the case of isotopic enrichment, the surface segregated layer can be described by an exponential function, as described by equation (2). Attempts to fit the surface excess profiles according to this exponential function gave decay lengths λ_d equal to 100 and 93 Å and powers in the exponent ξ of 6 and 5 respectively for the four- and five-layer fitting models. These values compare with the findings of Jones *et al.*[3], who obtained $\lambda_d = 243$ Å and $\xi = 1.56$ for the isotopic blend of dPS in PS. The discrepancies between the parameters reported by Jones *et al.*[3] and those obtained in this present work are evident. For the sample $\delta II\Delta_2$, therefore, surface segregation by isotopic enrichment mechanisms cannot be a true description of the segregation mechanism of dP(S-*b*-MMA) in PMMA. This can be rationalized by consideration of the adsorbing species, which in the case of PMMA will be dominated by the –C=O group, which would be largely unaffected by isotopic substitution. In this case there would be little or no difference in the surface energies of PMMA and dPMMA[3,4,12].

Copolymer micelle segregation

As discussed above, the surface segregation of copolymer micelles, due to the attractive interaction between the polymer brushes of the micelle and free surface, also produces a surface excess layer of copolymer[6,13]. Considering the sample $\delta II\Delta_2$, micelles forming a surface excess layer would consist of a dPS core and a dPMMA corona. These micelles must have formed when the copolymer in the PMMA homopolymer phase exceeds the critical micelle concentration (c.m.c.). At values of $\phi_c^{PMMA} \geqslant \phi_{cmc}$ the copolymers are able to aggregate into micelles, setting up a dynamic equilibrium between copolymers dissolved in bulk PMMA and those aggregated into micelles. The value of $\phi_c^{PMMA} = 0.055 \pm 0.005$, obtained from the four-layer fit model, therefore represents a lower limit on the value of the c.m.c. in the PMMA phase. Using the Leibler–Orland–Wheeler (LOW) theory[29], the value of ϕ_{cmc} can be calculated and gives $\phi_{cmc} \approx 0.04$*. This seems to be quite consistent with the experimentally observed value.

* It should be noted that, in calculating ϕ_{cmc} from the LOW theory, several assumptions must be made regarding the number of copolymer and homopolymer chains within the micelles, and therefore the value obtained can only be used as a guideline to the experimental observations

When the micelles form in the bulk PMMA, they experience an attractive interaction between their brushes and the free surface. This is associated with the entropy loss of homopolymer matrix chains in the vicinity of sharp interfaces[1]. The overall free energy of the system can be reduced by the micelles segregating to the free polymer surface and thereby decreasing the number of sharp interfaces in the system. In segregating to the surface the micelles create a brush profile, which can be modelled by modification of the hyperbolic tangent function of equation (1) to account for the large value of ϕ_c in the bulk PMMA to give:

$$\phi_c(z)=\left(\frac{1-\phi_c^{PMMA}}{2}\right)\left[1+\tanh\left(\frac{2(z_{offset}-z)}{w}\right)\right]+\phi_c^{PMMA} \quad (5)$$

The brush in this case derives from the PMMA corona of the micelles. The PMMA blocks that constitute the corona may be considered to be end-adsorbed to the PS cores, so that the brush wall becomes the average position of the tangents to the micelle core radii, as schematically illustrated in *Figure 6*. Assuming a brush wall position of $z=55$ Å for the experimental surface profiles of the four-layer model, and applying equation (5), gives a width factor $w=50$ for the best fit to the experimental data. Shull[22] has shown that w is a measure of the width over which the brush and matrix polymers overlap. The overlap is dependent on the radius of gyration of the brush, R_g^b, and ranges in magnitude from approximately $1.5R_g^b$ to $2.5R_g^b$, depending on the copolymer chemical potential. Under these circumstances, this gives R_g^b in the range 33 to 20 Å, which can be compared with a theoretical value[22] $R_g^b=a(N_b/6)^{1/2}=33$ Å, assuming a segment length of $a=6.85$ Å[30] and an average degree of polymerization of the PMMA brushes, $n_b=N_c/2=140$. The close agreement between values of R_g^b obtained from fits to experiment and those given by purely theoretical size considerations strongly suggests that surface segregation in sample δIIΔ_2 is indeed a result of micelle formation.

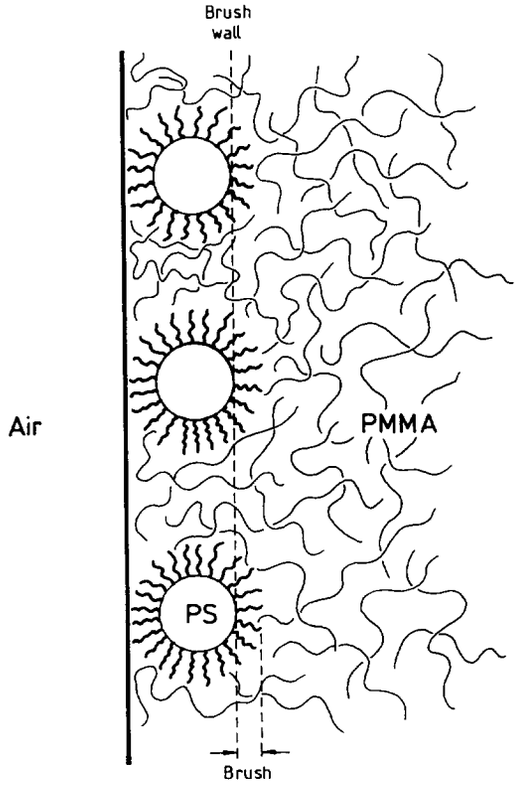

Figure 6 Schematic illustration of a surface segregated layer of copolymer micelles, showing the average position of the brush wall from which the brush extends into the bulk PMMA phase

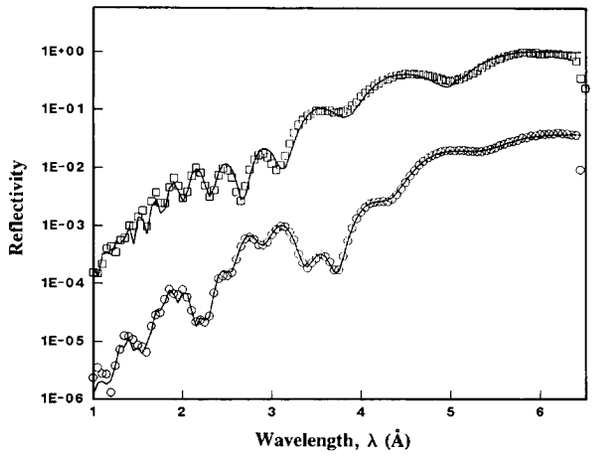

Figure 7 Reflectivity *versus* wavelength profiles of sample εII a.m. (○) and after 250 min annealing at 150°C (□). The full curves superimposed on the data represent the best-fit simulated profiles using the fitting models plotted in *Figure 8*

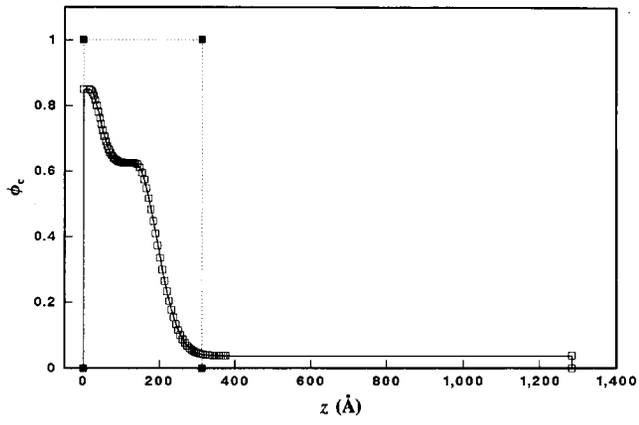

Figure 8 The $\phi_c(z)$ profiles used to produce the simulated reflectivity profiles in *Figure 7* for sample εII a.m. (■) and after 250 min annealing (□)

Imitating surface segregation

The surface excess behaviour observed by sample δIIΔ_2 can be further investigated using sample εII (see *Table 2*). Here the copolymer at the air/polymer interface is allowed to diffuse into the bulk PMMA during annealing at 150°C. The reflectivity *versus* wavelength profiles for the a.m. sample (circles) and after 250 min annealing (squares) are shown in *Figure 7*, upon which are superimposed full curves representing the best fits obtained from the fitting procedures.

The analysed reflectivity data of sample εIIΔ_1 indicate that mutual diffusion of dP(S-*b*-MMA)28 and PMMA has resulted in a three-layer step profile, with copolymer found throughout the thickness of the sample. The ϕ_c *versus* z profile was obtained by applying equation (4) to the fitting data to give the profiles shown in *Figure 8* by the open squares. The step profile between the air/polymer and bulk PMMA layers is now evident, with a copolymer surface volume fraction $\phi_s=0.849\pm0.042$,

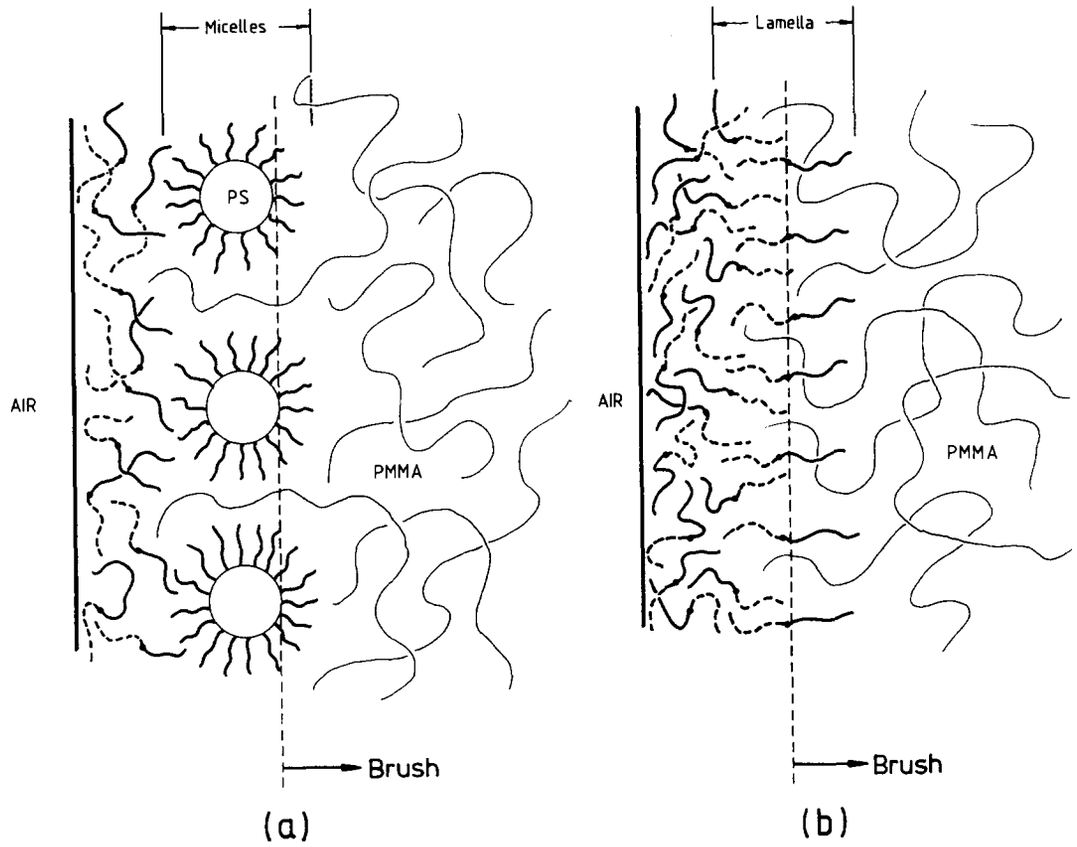

Figure 9 Schematic illustration of surface segregated layers of (a) copolymer micelles and (b) lamella, formed during mutual diffusion of initially pure layers of PMMA and a surface layer of dP(S-*b*-MMA)

which falls via a step located at $136 \leqslant z\,(\text{Å}) \leqslant 376$ with a value of $\phi_c = 0.623 \pm 0.010$, eventually dropping to the value in the PMMA phase of $\phi_c^{PMMA} = 0.038 \pm 0.010$ at z values greater than 376 Å.

The step profile must be caused through the action of mutual diffusion between the PMMA homopolymer and dP(S-*b*-MMA)28 copolymer chains. The PMMA diffusing into the pure copolymer layer will act as a high-molecular-weight solvent. This will have the effect of causing the copolymers to rearrange their morphologies in order to reduce the contacts of their PS segments with the PMMA matrix chains. The copolymer can achieve this by forming either micelles or lamellar microphase-segregated layers. These structures are shown schematically in *Figure 9*. Before equilibrium is reached, the copolymers (as either micelles or lamella) will be in a dynamic situation with free copolymer chains diffusing into the bulk PMMA, while being fed from the free surface saturated copolymer layer. Simultaneously, the PMMA matrix chains diffuse in the opposite direction to accommodate the copolymer within the bulk polymer layer. The net result of this mutual diffusion process is that the free surface saturated copolymer layer reduces in thickness with annealing, and the micelle/lamella microphase-separated layer appears to move towards the free surface. At equilibrium, this mutual diffusion process between the copolymer and homopolymer will ultimately lead to a free surface segregated layer of microphase-separated copolymer. This situation would then be equivalent to that observed in sample $\delta\text{II}\Delta_2$, where copolymer diffused from some distant position to produce a free surface segregated excess copolymer layer.

In the $\varepsilon\text{II}\Delta_1$ sample, for both micellar and lamellar structures, dPMMA chains of the copolymer will behave as end-tethered brushes, in which case the $\phi_c(z)$ step profile will be described by the hyperbolic tangent function of equation (5). A best fit to the experimental $\phi_c(z)$ profile using equation (5) is obtained when $w = 100$, giving R_s^b in the range of 67 to 40 Å. This compares to the theoretical value of $R_g^b = 33$ Å.

These arguments about copolymer micelle/lamella layer formation will equally apply to the step profile formed near the substrate in sample $\delta\text{II}\Delta_2$. Here, again, mutual diffusion of the PMMA matrix and dP(S-*b*-MMA)28 copolymer chains creates a copolymer ordered layer in a dynamic situation with the two essentially pure polymer layers on either side. Fits to the $\delta\text{II}\Delta_2\,\phi_c(z)$ profile using the hyperbolic tangent function of equation (5) gives a width factor of $w = 50$ and consequently values of $R_g^b = 33$ to 20 Å.

CONCLUSIONS

Determination of volume fraction as a function of depth normal to the sample surface was achieved by model fitting to the neutron reflectivity curves. In this way the copolymer segregation behaviour can be observed. The copolymer segregation behaviour is influenced by the nature of the interfaces present within the system.

Free surface copolymer segregation is most likely to occur as a result of the copolymer microphase segregating into either lamellae or micelles. These structures then segregate to the air/polymer interface, since there is a thermodynamic driving force that favours this free surface

segregation by these copolymer assemblies. The packing of the copolymers at the free surface produces a copolymer brush profile characteristic of end-tethered polymers. The shape of the brushes is well described by theoretical predictions of brush behaviour and allows estimation of brush radii of gyration. By curve fitting to the experimental brush profiles, it is observed that the brush radii of gyration are of the order of half that of the total copolymer. This brush formation associated with copolymer microphase segregation is also observed as a result of mutual diffusion between initially pure layers of copolymer and homopolymer, and is the cause of steps in the volume fraction–depth profiles. The tails of these steps can be fitted to theoretical brush profiles, indicating formation of copolymer microphase structures.

ACKNOWLEDGEMENTS

The authors gratefully acknowledge the help of Dr M. L. Fernandez for experimental assistance. In addition we wish to thank ICI plc for their financial support of this work in the form of a studentship for DGB.

REFERENCES

1 Shull, K. R., Winney, K. I., Thomas, E. L. and Kramer, E. J. *Macromolecules* 1991, **24**, 2748
2 Jones, R. A. L., Kramer. E. J., Rafailovich, M. H., Sokolov, J. and Schwarz, S. A. *Phys. Rev. Lett.* 1989, **62**, 280
3 Jones, R. A. L., Norton, L. J., Kramer, E. J., Composto, R. J., Stein, R. S., Russell, T. P., Mansour, A., Karim, A., Felcher, G. P., Rafailovich, M. H., Sokolov, J., Zhao, X. and Schwarz, S. A. *Europhys. Lett.* 1990, **12**, 41
4 Jones, R. A. L. and Kramer, E. J. *Phil. Mag.* (*B*) 1990, **62**, 129
5 Bates, F. S., Wignall, G. D. and Koehler, W. C. *Phys. Rev. Lett.* 1986, **55**, 932
6 Mills, P. J., Green, P. F., Palmstrom, C. J., Mayer, J. W. and Kramer, E. J. *Appl. Phys. Lett.* 1984, **45**, 957
7 Payne, R. S., Clough, A. S., Murphy, P. and Mills, P. J. *Nucl. Instrum. Meth. Phys. Res.* (*B*) 1989, **42**, 130
8 Bates, F. S. *Macromolecules* 1985, **18**, 525
9 Higgins, J. S. *Makromol. Chem., Macromol. Symp.* 1988, **15**, 201
10 Benoit, H., Cotton, J. P., Decker, D., Farnoux, B., Higgins, J. S., Jannick, G., Ober, R. and Picot, P. *Nature* (*London*) 1973, **245**, 13
11 Bates, F. S., Berney, C. V., Cohen, R. E. and Wignall, G. D. *Polymer* 1983, **24**, 519
12 Leonhardt, D. C., Johnson, H. E. and Granick, S. *Macromolecules* 1990, **23**, 685
13 Shull, K. R., Kramer, E. J., Hadziioannou, G. and Tang, W. *Macromolecules* 1990, **23**, 4780
14 Turos, A. and Meyer, O. *Nucl. Instrum. Meth.* 1984, **232**, 92
15 Dieumegard, D., Dubreuil, D. and Amsel, G. *Nucl. Instrum. Meth.* 1979, **166**, 431
16 Benninghoven, A., Rudenaur, F. G. and Werner, H. W. 'Secondary Ion Mass Spectroscopy', Chemical Analysis Series, Vol. 86, Wiley, New York, 1987
17 Penfold, J. and Thomas, R. K. *J. Phys., Condens. Matter* 1989, **2**, 1369
18 Russell, T. P. *Mater. Sci. Rep.* 1990, **5**, 171
19 Lekner, J. 'Theory of Reflection', Martinus Nijhoff, Dordrecht, 1987
20 Penfold, J. *J. Phys.* (*Paris*) 1989, **50**, C7
21 Heavens, O. S. 'Optical Properties of Thin Films', Butterworths, London, 1955
22 Shull, K. R. *J. Chem. Phys.* 1991, **94**, 5723
23 Kinning, D. J., Thomas, E. L. and Fetters, L. J. *J. Chem. Phys.* 1989, **90**, 5806
24 Shull, K. R. and Kramer, E. J. *Macromolecules* 1990, **23**, 4769
25 Bartell, L. S. and Roskos, R. R. *J. Chem. Phys.* 1966, **44**, 457
26 Penfold, J., Ward, R. C. and Williams, W. G. *J. Phys.* (*E*) *Sci. Instrum.* 1987, **20**, 1411
27 Crank, J. 'The Mathematics of Diffusion', 2nd Edn., Oxford University Press, Oxford, 1975
28 Bucknall, D. G., PhD Thesis, Imperial College, 1991
29 Leibler, L., Orland, H. and Wheeler, J. C. *J. Phys. Chem.* 1983, **79**, 3550
30 Russell, T. P., Anastasiadis, S. H., Menelle, A., Felcher, G. P. and Satja, S. K. *Macromolecules* 1991, **24**, 1575